BiOCl Decorated NaNbO$_3$ Nanocubes: A Novel p-n Heterojunction Photocatalyst With Improved Activity for Ofloxacin Degradation

Jingjing Xu [1]*, Bingbing Feng [1], Ying Wang [1], Yadi Qi [1], Junfeng Niu [2] and Mindong Chen [1]

[1] Jiangsu Key Laboratory of Atmospheric Environment Monitoring and Pollution Control, School of Environmental Science and Engineering, Collaborative Innovation Center of Atmospheric Environment and Equipment Technology, Jiangsu Engineering Technology Research Center of Environmental Cleaning Materials, Nanjing University of Information Science and Technology, Nanjing, China, [2] Research Center for Eco-Environmental Engineering, Dongguan University of Technology, Dongguan, China

BiOCl/NaNbO$_3$ p-n heterojunction photocatalysts with significantly improved photocatalytic performance were fabricated by a facile *in-situ* growth method. The obtained BiOCl/NaNbO$_3$ samples were characterized by UV-vis absorption spectroscopy, scanning electron microscopy (SEM), X-ray diffraction (XRD), photocurrent (PC) and photoluminescence spectroscopy (PL). The photocatalytic activity of the BiOCl/NaNbO$_3$ samples was investigated by the degradation of a typical antibiotic Ofloxacin (OFX). The experimental results showed that BiOCl/NaNbO$_3$ composites exhibited much higher photocatalytic activity for OFX degradation compared to pure NaNbO$_3$ and BiOCl. The degradation percent of OFX reached 90% within 60 min, and the apparent rate constant was about 8 times as that of pure NaNbO$_3$ and BiOCl. The improved activity can be attributed to the formation of p-n junction between NaNbO$_3$ and BiOCl. The formed p-n junction facilitated the separation of photogenerated holes and electrons, thereby enhancing photocatalytic activity. In addition, the composite photocatalyst showed satisfactory stability for the degradation of OFX. Due to the simple synthesis process, high photocatalytic activity, and the good recyclability of these composite photocatalysts, the results of this study would provide a good example for the rational design of other highly efficient heterojunction photocatalytic materials.

Keywords: photocatalysis, BiOCl, NaNbO$_3$, p–n junction, ofloxacin

INTRODUCTION

The problem of water pollution has attracted increasing attention worldwide due to many toxic pollutants continue to enter into our water bodies (Ao et al., 2016b; Li et al., 2018; Yuan et al., 2018). As a green and sustainable technology, semiconductor photocatalysis can completely eliminate most pollutants in water and air (Zhang et al., 2016, 2017a,b; Chen et al., 2018; Guo et al., 2018; He et al., 2018; Yang et al., 2018). The contaminants are degraded by hydroxyl radical or other free

radicals which are produced in the process after the absorption of light (Li et al., 2015; Cao et al., 2016; Xu et al., 2016; Yu et al., 2016; Zhang and Xiao, 2017; Han et al., 2018; Zhong et al., 2018). There are many semiconductors (such as oxides, sulfides, nitrates and silver based compounds etc.) can be served as photocatalysts to induce the degradation of pollutants.

In recent years, $NaNbO_3$ has attracted much attention due to its unique properties of nonlinear optics, ferroelectric, ionic conduction, photorefractive and photocatalytic properties (Katsumata et al., 2010; Lv et al., 2010; Li et al., 2012a, 2013; Fan et al., 2015; Qian et al., 2018). Because $NaNbO_3$ is a typical n type semiconductor with unique crystal [NbO6] angle eight-hedral crystal structure, it has the advantage of relative high transfer efficiency of electrons during the photocatalytic process (Shi et al., 2014b; Song et al., 2015). Recent studies have shown that $NaNbO_3$ can be used as an efficient photocatalyst for the evolution of H_2 and the reduction of CO_2 (Li et al., 2012b, 2014). In addition, $NaNbO_3$ also shows the ability for the decomposition of organic pollutants (Li et al., 2008; Li, 2010; Chen et al., 2014). However, because $NaNbO_3$ has a large band-gap, it cannot be used as a visible light responsive photocatalyst. Various experiments have shown that forming heterojunction with other semiconductor materials was a promising way to improve the photocatalytic activity of $NaNbO_3$. For example, an effective composite photocatalyst $NaNbO_3/WO_3$ has been proved to has stronger dye degradation activity compared with the corresponding single component (Shifu et al., 2013). Moreover, other $NaNbO_3$ based composite photocatalysts, such as $AgO_2/NaNbO_3$ (Zhang et al., 2017), $Pt/NaNbO_3$ (Liu et al., 2016) and $CdS/NaNbO_3$ (Kumar et al., 2014), were also successfully prepared for photocatalytic degradation of pollutants.

On the other hand, although BiOCl (a typical p-type oxyhalide semiconductor) has been extensively investigated in the field of photocatalysis (Ye et al., 2014; Ao et al., 2016a; Hu et al., 2016; Mao et al., 2016; Ma Y. C. et al., 2016; Wang et al., 2018). However, the recombination rate of photogenerated charges in pure phase of BiOCl is high, resulting in its limited photocatalytic activity under UV light. It has recently been found that the photocatalytic activity of BiOCl can be promoted through the formation of p-n junctions with n type semiconductors (Rajeshwar et al., 2001; Wang et al., 2012; Fang et al., 2016). The enhanced activity can be ascribed to the fact that the internal electric field at the p-n junction interface improved the separation and transfer of photo-generated charges (Yan et al., 2017). However, as far as we know, the preparation and activity of BiOCl/$NaNbO_3$ p-n heterojunction photocatalyst have not been studied yet.

In the present work, we constructed a new type of p-n heterojunction photocatalyst (BiOCl/$NaNbO_3$) by a simple *in situ* growth method. Compared with pure BiOCl and $NaNbO_3$, the composite has better photocatalytic activity for the degradation of ofloxacin (OFX). The experimental results proved that the p-n junctions formed between BiOCl/$NaNbO_3$ composites promote the transfer and separation of photogenerated electron-hole pairs, thus enhancing the photocatalytic activity.

EXPERIMENTAL

Synthesis of NaNbO₃ Cubes

All the reagents and materials used in this experiment were analytical grades. All of them were purchased from China pharmaceutical chemical reagents Co., Ltd. $NaNbO_3$ was directly synthesized by hydrothermal method described as following. 2 g Nb_2O_5 was added to the 120 mL NaOH solution (10 M) and stirred for 120 min before the suspension was transferred to the 200 ml Teflon-lined stainless steel autoclave. The reaction kettle was kept at 150°C for 48 h. Subsequently, the autoclave was cooled to room temperature naturally after the reaction. Then remove the reactor and precipitate it naturally, pour the supernatant out of the precipitate and centrifugate, then wash it with deionized water and ethanol for 3–5 times. Finally, the product was dried for 12 h in a vacuum oven at 60°C.

Synthesis of BiOCl/NaNbO₃ p–n Junction Photocatalysts

BiOCl/$NaNbO_3$ heterostructures were prepared by a simple *in-situ* growth method. A certain amount of $Bi(NO_3)_3 \cdot 5H_2O$ was added to 300 mL of ultrapure water and stirred for 1 h to form solution A. Meanwhile, $NaNbO_3$ powder was dispersed in 80 mL ultrapure water and sonicated for 30 min to form solution B. A certain amount of KCl was added to 60 mL ultrapure water to form solution C. Finally, B and C were slowly added to A under rapid stirring. Afterwards, the stirring was continued for 24 h. The product was then filtered and thoroughly washed with distilled water and ethanol before it was dried at 60°C for 24 h. By Changing the amount of $Bi(NO_3)_3 \cdot 5H_2O$ and KCl added, $NaNbO_3$/BiOCl composites with different theoretical BiOCl mass ratios of 10, 25, 75, and 100% (expressed as BN-1, BN-2, BN-3, and BN-4) were produced. In order to facilitate comparison, pure BIOCl samples are also prepared in the same way, that is to say, no $NaNbO_3$ is added in the process of making composite samples.

Characterization of Photocatalysts

The results of X ray diffraction (XRD) scanning of pure BiOCl, $NaNbO_3$ and BiOCl/$NaNbO_3$ were recorded by Shimadzu XRD 6100 X-ray diffractometer. The morphology and microstructure of the samples were characterized by scanning electron microscopy (SEM, Hitach S-4800). The band gap (Eg) of the sample was measured by UV-vis absorption spectroscopy at 200~800 nm at room temperature, and the integrated ball attachment was installed on the ultraviolet visible spectrophotometer (UV-3600). Photocurrent (PC) and mott-Schottky (MS) were carried out on the traditional three electrode system (the electrochemical workstation of CHI-660D Chenhua chemical equipment company in Shanghai, China). The contrast electrode and the reference electrode are platinum electrodes and Ag/AgCl electrodes respectively.
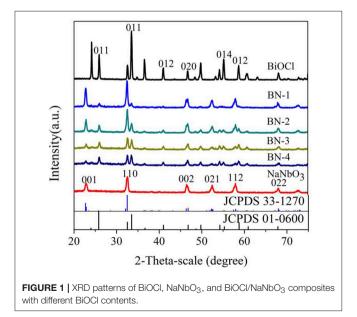
Photocatalytic Activity Experiments

The experimental vessel is a double-layer quartz beaker with cooling water circulation system for photocatalytic reaction. During the experiment, the temperature of the solution can

be maintained at about 25 °C, so as to reduce the influence of temperature on the experiment. The light source used in the photocatalytic process is a 300 W xenon lamp(200 nm<λ<400 nm), and before irradiation, 25 mg photocatalyst was added to 50 mL OFX solution (5 mg/L). The suspension was stirred magnetically in the dark for 30 min to achieve adsorption/desorption equilibrium between photocatalysts and OFX. During the photocatalytic process, a certain suspension was sampled at the prescribed time intervals. The sampled suspension was centrifuged before the determination of OFX concentration.

RESULTS AND DISCUSSION

Characterizations

The XRD diagrams of pure BiOCl, NaNbO$_3$ and BiOCl/NaNbO$_3$ composites were shown in **Figure 1**. It can be seen that there are seven different diffraction peaks, which can be indexed to tetragonal BiOCl (JCPDS card number 01-0600) (Ma W. et al., 2016). Sharp and narrow diffraction peaks indicate good crystallinity for pure BiOCl. From the pattern of pure NaNbO$_3$, several main diffraction peaks can be seen at 22.7, 32.5, 46.4, 52.7, 58.1, and 68.11° corresponding to (001), (110), (002), (021), (112), and (022) planes of NaNbO$_3$ orthorhombic phases (JCPDS card number 33-1270) (Saito and Kudo, 2013). The diffraction peaks of pure BiOCl and NaNbO$_3$ and the diffraction peaks of heterostructure BiOCl/NaNbO$_3$ composites can be clearly observed by XRD diagram. In addition, when the mass ratio of BiOCl to NaNbO$_3$ increases from 10 to 100%, the diffraction peak intensity of BiOCl increases and the corresponding NaNbO$_3$ peak intensity decreases. Furthermore, when BiOCl grows on NaNbO$_3$, its diffraction peak is wider than that of pure BiOCl. This phenomenon indicates that BiOCl on the surface of NaNbO$_3$ cube has smaller particle size. The result indicates that the addition of NaNbO$_3$ can effectively inhibit the growth of BiOCl (Shang et al., 2009). XRD showed that the samples were

clean and had no other phase of impurity, so the composites were basically composed of BiOCl and NaNbO$_3$.

The morphology and structure of BiOCl, NaNbO$_3$, and BiOCl/NaNbO$_3$ composites can be clearly seen by SEM characterization. The SEM image of pure BiOCl is displayed in **Figure 2a**. As can be seen from the graph, pure BiOCl is composed of regular, square like nano plates. At the same time, we can see that the synthesized NaNbO$_3$ has irregular cubic shape and smooth surface in **Figure 2b**. A typical SEM image of the BN-3 composite is shown in **Figure 2c**. It can be seen that NaNbO$_3$ cubes are anchored by BiOCl nanosheets which are thiner and smaller than pure BiOCl. During the in-sith growth process, the NaNbO$_3$ particles played a role of heterogeneity and inhibited the
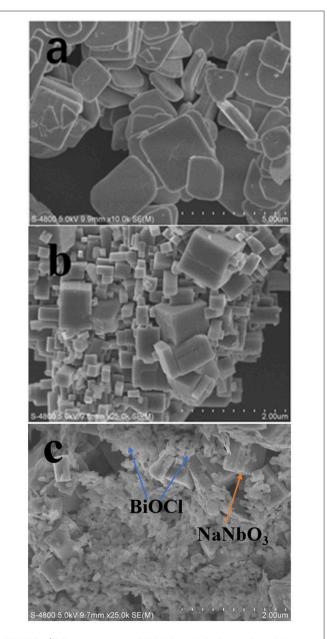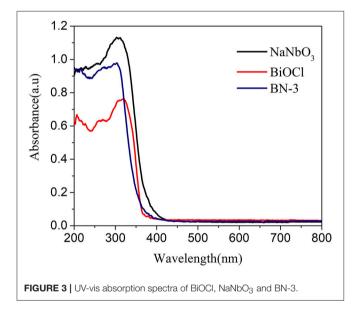

FIGURE 1 | XRD patterns of BiOCl, NaNbO$_3$, and BiOCl/NaNbO$_3$ composites with different BiOCl contents.

FIGURE 2 | SEM images of pure BiOCl **(a)**, NaNbO3 **(b)** and BN-3 **(c)**.

growth of BiOCl to lager ones. After analyzing the SEM image, the conclusion is in good agreement with the previous XRD analysis. BiOCl and NaNbO$_3$ form p-n junctions at the interface because of the close contact between BiOCl and NaNbO$_3$. This improves the carrier transport rate and separation efficiency in photocatalysis and helps to improve the activity.

The optical properties of the samples have a great influence on the utilization of sunlight. Therefore, UV-DRS for pure BiOCl, NaNbO$_3$ and BiOCl/NaNbO$_3$ composites are investigated. As we can see from **Figure 3**, the absorbance threshold of NaNbO$_3$ and pure BiOCl are at about 400 and 380 nm, respectively. The band-gap of photocatalysts can be obtained from the following equation:

$$Eg = 1240/\lambda,$$

where Eg is the band-gap energy and λ is the cut off wavelength. Therefore, the band gaps of NaNbO$_3$ and BiOCl prepared were 3.10 and 3.26 eV, respectively, which are similar to those reported previously (Shi et al., 2014a; Ma W. et al., 2016). It can also be seen

FIGURE 3 | UV-vis absorption spectra of BiOCl, NaNbO$_3$ and BN-3.

from **Figure 3** that BiOCl/NaNbO$_3$ exhibits higher UV absoption performance compared to pure BiOCl. Furthermore, the band edge of BiOCl/NaNbO$_3$ exhibits a little red shift compared to pure BiOCl.

Through the band structure of the catalyst, we further explore the way of carrier transfer. The type and surface potential of NaNbO$_3$ and BiOCl semiconductors are determined by the Mott-Schottky plots. The positive tangent in the graph indicates that the sample is n type semiconductor, while the negative tangent in the graph indicates that the sample is p type semiconductor (Kuang et al., 2015). The results shown in **Figures 4A,B** show that BiOCl and NaNbO$_3$ are p-type and n-type semiconductors, respectively. In addition, the flat potential (relative to Ag/AgCl) of BiOCl and NaNbO$_3$ are 2.30 V and −0.70 V respectively through the intersection point between tangent and abscissa. According to the following equation, the potential (relative to Ag/AgCl) can be converted to a normal hydrogen electrode (NHE). (1) (Zhou et al., 2017; Liu et al., 2018):
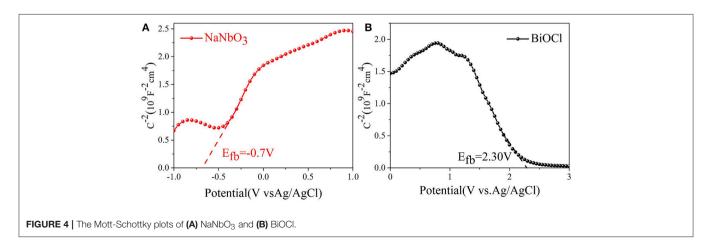
$$E_{NHE} = E_{Ag/AgCl} + E^0_{Ag/AgCl}$$

where $E^0_{Ag/AgCl} = 0.197$ V. In particular, the maximum of the valence band (VB) is about 0.1 V lower than the flat potential of the p-type semiconductor; the minimum value of the conduction band (CB) is about 0.1 V higher than the flat potential of the n-type semiconductor (Liu et al., 2017b). Therefore, the VB position of BiOCl and the CB position of NaNbO$_3$ are 2.60 and −0.60 V (vs. NHE), respectively. The Eg of BiOCl and NaNbO$_3$ were 3.26 and 3.10, respectively. Therefore, according to Eg. (2) (Liu et al., 2017a):

$$Eg = E_{VB} - E_{CB}$$

the position of CB and VB for BiOCl and NaNbO$_3$ are −0.66 and 2.50 V, respectively.

Photocatalytic Activity

The photocatalytic activity of BiOCl/NaNbO$_3$ composites with p-n junctions is mainly studied on the degradation of OFX under UV irradiation. As shown in **Figure 5A**, In the presence of NaNbO$_3$ or BiOCl, about 20% OFX are decomposed within
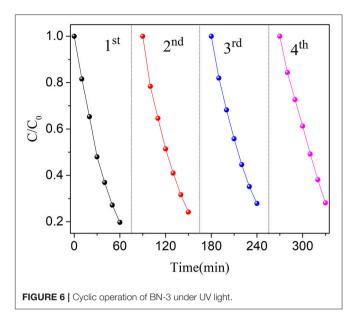

FIGURE 4 | The Mott-Schottky plots of **(A)** NaNbO$_3$ and **(B)** BiOCl.

60 min. It can also be seen that all BiOCl/NaNbO$_3$ composites exhibit significantly higher photocatalytic activity than that of pure BiOCl and NaNbO$_3$. In addition, it was found that the mass ratio of BiOCl has a significant effect on the activity of BiOCl/NaNbO$_3$ composites. Specifically, the activity increase gradually when the BiOCl content is increased from 10 to 75%. When the content of BiOCl is further increased to 100%, the activity of the sample begin to decrease. Therefore, sample BN-3 with BiOCl mass ratio of 75% exhibites the highest activity (the degradation percent of OFX is about 90% after 60 min irradiation). The time evolution of the OFX solution spectra in the degradation process by BN-3 were measured and are shown in **Figure 5B**. The absorption peak of OFX decreases as the increase of irradiation time and reaches the minimum at 60 min.

It has also been found that the photocatalytic degradation of OFX follows pseudo-first order kinetic calculated from the following formula (as shown in **Figure 5C**):

$$-\ln(C_t/C_0) = kt$$

The obtained k of OFX removal rate of pure BiOCl, NaNbO$_3$ and BiOCl /NaNbO$_3$ composites can be calculated by this formula. In **Figure 5D**, it is more clear to see that the kinetic constants of BiOCl, NaNbO$_3$, BN-1, BN-2, BN-3, and BN-4 are 0.0021, 0.002, 0.0071, 0.0094, 0.016, and 0.011 min^{-1}, respectively.

Therefore, compared with the single phase BiOCl and NaNbO$_3$, the BiOCl/NaNbO$_3$ composite can promote the separation of the electron-hole pairs on the interface, thus promoting the enhancement of the photocatalytic activity.
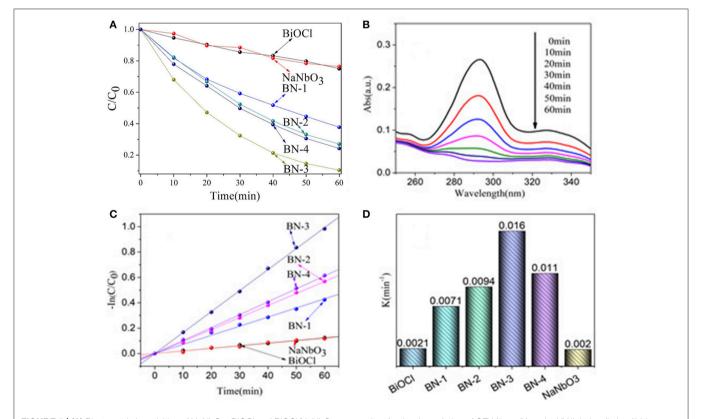

FIGURE 6 | Cyclic operation of BN-3 under UV light.

FIGURE 5 | (A) Photocatalytic activities of NaNbO$_3$, BiOCl and BiOCl/NaNbO$_3$ composites for the degradation of OFX (5 mg/L) under UV light irradiation (200 nm < λ <400 nm), **(B)** UV spectral changes of OFX in aqueous BN-3 composites dispersions as a function of irradiation time, **(C)** The kinetics of OFX degradation, and **(D)** The degradation rateconstants.

The stability of one photocatalyst is very important to the practical application. Therefore, the recycle experiments are carried out for BN-3. As shown in **Figure 6**, the photocatalytic performance of the catalyst has only slight loss after four cycles of reutilization of the photocatalyst. This experimental phenomenon indicates that the photocatalyst is stable to the photodegradation of OFX. The experimental results show that the photocatalytic degradation of organic pollutants by the prepared BiOCl/NaNbO$_3$ composites is stable, and it is of great significance for the practical application of the catalyst.

Photocatalytic Mechanism

The interfacial charge transfer kinetics between BiOCl and NaNbO$_3$ can be further elucidated by photocurrent measurements. **Figure 7** shows the photocurrent-time curves of the BiOCl, NaNbO$_3$, and BN-3 composites under an on/off cycle of intermittent UV irradiation. As shown in **Figure 7**, BN-3 composite exhibits much higher photocurrent than
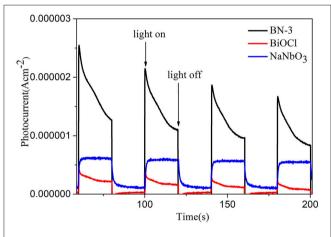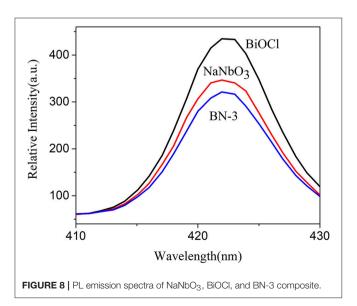
that of pure BiOCl and NaNbO$_3$. Therefore, the BN-3 can transfer and separate photogenerated electron hole pairs more efficiently under ultraviolet light irradiation. In addition, the photoluminescence (PL) spectra of pure BiOCl, NaNbO$_3$ and BiOCl/NaNbO$_3$ composite samples were tested to determine the separation efficiency of photo-generated charges. The excitation wavelength used in the test is 285 nm. In **Figure 8**, it is found that pure NaNbO$_3$ is the strongest relative to other sample emission peaks within the range of 350–550 nm. For pure BiOCl samples, their emission peaks are relatively weak relative to pure NaNbO$_3$. The PL luminescence strength of BN-3 composites is the lowest in the three samples. The results show that the combination of pure BiOCl and NaNbO$_3$ can effectively inhibit the recombination of electron hole pairs. The results are in good agreement with the measurement results of photocurrent.

In order to study the degradation mechanism, the main active species produced in the degradation process were determined. Therefore, three radical scavengers such as isopropanol (IPA, •OH scavenger) (Cao et al., 2012), ammonium oxalate (AO, h$^+$ scavenger) (Chang et al., 2013) and p-benzoquinone (BQ, •O$_{2-}$ scavenger) (Sun et al., 2017) have been added separately in the degradation systems. When BQ and AO were introduced, the degradation rate of OFX decreased significantly (see **Figure 9**). Moreover, the degradation rate of OFX was also decreased in the presence of IPA. These results indicate that h$^+$ and •O$_{2-}$ play an important role in the degradation process. •OH has a certain effect on the degradation of OFX. Therefore, we can conclude that the free radicals of •O$_{2-}$, h$^+$ and •OH in active species play a certain role in the degradation of OFX.

The formation of heterojunction in the composite system has a positive effect on the separation of photogenerated electrons and holes. Based on the above experimental results, we propose a reasonable photocatalytic mechanism for BiOCl/NaNbO$_3$ (**Scheme 1**). The enhanced photocatalytic activity of BiOCl/NaNbO$_3$ heterojunction originates from the
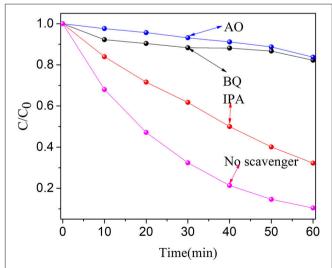

FIGURE 7 | Transient photocurrent responses for NaNbO$_3$, BiOCl, and BN-3 composite.

FIGURE 8 | PL emission spectra of NaNbO$_3$, BiOCl, and BN-3 composite.

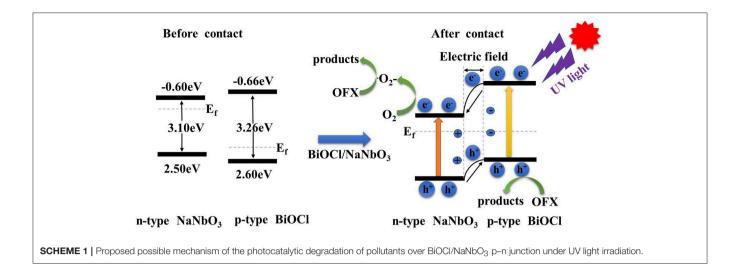**FIGURE 9 |** Trapping experiment of active species during the photocatalytic degradation of OFX over BN-3 under UV light irradiation.

SCHEME 1 | Proposed possible mechanism of the photocatalytic degradation of pollutants over BiOCl/NaNbO$_3$ p–n junction under UV light irradiation.

unique matching band location of these two semiconductors after forming heterojunction. Based on the experimental data, we know that the band gap of BiOCl is larger than that of NaNbO$_3$. The Fermi level (E_f) of BiOCl is located near the valence band because it is a p type semiconductor, and the Fermi level of n type semiconductor NaNbO$_3$ approaches the conduction band. When the mixture of BiOCl and NaNbO$_3$ forms a p-n type heterojunction of BiOCl/NaNbO$_3$, the Fermi level of BiOCl moves upwards, while the Fermi level of the NaNbO$_3$ moves downward until the Fermi level of BiOCl and NaNbO$_3$ is at the same level. Finally, the CB position of BiOCl becomes higher than NaNbO$_3$ after moving up. At the same time, BiOCl and NaNbO$_3$ form an internal electric field in the final equilibrium state. At the same time, the valence band (VB) of NaNbO$_3$ is also lower than that of BiOCl. Due to the special band structure of the BiOCl/NaNbO$_3$ composite, the photoelectrons are excited from the VB of the BiOCl to the CB, because the special ladder like structure of the BiOCl/NaNbO$_3$ heterostructure leads to the electronic transfer from CB of BiOCl to the CB of NaNbO$_3$. Electrons stored in NaNbO$_3$'s CB can react with dissolved O$_2$ to form •O$_2^-$, while the adsorbed hydroxy or H$_2$O molucules can also react with h$^+$ to form •OH or directly oxidize organic pollutants. Therefore, the formed p-n junction between BiOCl and NaNbO$_3$ provide an effective electron transfer path to reduce the recombination of electron-hole pairs, thus improving the activity of the as fabricated BiOCl/NaNbO$_3$ composites.

CONCLUSIONS

In this work, BiOCl/NaNbO$_3$ composites with p-n heterojunctions were synthesized by simple hydrothermal method. Through experiments and characterization, it is confirmed that p-n junctions formed on the interface between BiOCl and NaNbO$_3$. The results indicted that the separation efficiency of photo-generated carriers has been greatly improved because of the formation of p-n junctions. Recycle experiments showed that the composite photocatalyst exhibited good stability. The experimental results also show that pollutants are mainly degraded by h$^+$ and •O$_2^-$ radicals. Therefore, BiOCl/NaNbO$_3$ heterojunction nanocomposites can be used as a highly efficient and reusable photocatalyst, which has potential applications in the removal of organic pollutants.

AUTHOR CONTRIBUTIONS

JX and MC designed the project, guided the study and polished the manuscript. BF, YW, and YQ conducted the experiments and characterized the samples. JN revised the manuscript.

ACKNOWLEDGMENTS

REFERENCES

Ao, Y. H., Bao, J. Q., Wang, P. F., Wang, C., and Hou, J. (2016a). Bismuth oxychloride modified titanium phosphate nanoplates: a new p-n type heterostructured photocatalyst with high activity for the degradation of different kinds of organic pollutants. *J. Colloid Interface Sci.* 476, 71–78. doi: 10.1016/j.jcis.2016.05.021

Ao, Y. H., Wang, K. D., Wang, P. F., Wang, C., and Hou, J. (2016b). Synthesis of novel 2D-2D p-n heterojunction BiOBr/La$_2$Ti$_2$O7 composite photocatalyst with enhanced photocatalytic performance under both UV and visible light irradiation. *Appl. Catal. B Environ.* 194, 157–168. doi: 10.1016/j.apcatb.2016.04.050

Cao, J., Xu, B. Y., Lin, H. L., Luo, B. D., and Chen, S. F. (2012). Novel Bi2S3-sensitized BiOCl with highly visible light photocatalytic activity for the removal of rhodamine B. *Catal. Commun.* 26, 204–208. doi: 10.1016/j.catcom.2012.05.025

Cao, M., Wang, P., Ao, Y., Wang, C., Hou, J., and Qian, J. (2016). Visible light activated photocatalytic degradation of tetracycline by a magnetically separable composite photocatalyst: graphene oxide/magnetite/cerium-doped titania. *J. Colloid Interface Sci.* 467, 129–139. doi: 10.1016/j.jcis.2016.01.005

Chang, C., Zhu, L. Y., Fu, Y., and Chu, X. L. (2013). Highly active Bi/BiOI composite synthesized by one-step reaction and its capacity to degrade bisphenol A under simulated solar light irradiation. *Chem. Eng. J.* 233, 305–314. doi: 10.1016/j.cej.2013.08.048

Chen, P., Dong, F., Ran, M. X., and Li, J. R. (2018). Synergistic photo-thermal catalytic NO purification of MnOx/g-C$_3$N$_4$: enhanced performance and reaction mechanism. *Chin. J. Catal.* 39, 619–629. doi: 10.1016/S1872-2067(18)63029-3

Chen, S. F., Hu, Y. F., Ji, L., Jiang, X. L., and Fu, X. L. (2014). Preparation and characterization of direct Z-scheme photocatalyst Bi$_2$O$_3$/NaNbO$_3$ and its reaction mechanism. *Appl. Surf. Sci.* 292, 357–366. doi: 10.1016/j.apsusc.2013.11.144

Fan, M. S., Hu, B., Yan, X., Song, C. J., Chen, T. J., Feng, Y., et al. (2015). Excellent visible-light-driven photocatalytic performance of Cu$_2$O sensitized NaNbO$_3$ heterostructures. *New J. Chem.* 39, 6171–6177. doi: 10.1039/C5NJ00751H

Fang, S. S., Ding, C. Y., Liang, Q., Li, Z. Y., Xu, S., Peng, Y. Y., et al. (2016). *In situ* precipitation synthesis of novel BiOCl/Ag$_2$CO$_3$ hybrids with highly e?cient visible-light-driven photocatalytic activity. *J. Alloy. Compd.* 684, 230–236. doi: 10.1016/j.jallcom.2016.05.168

Guo, Y., Wang, P. F., Qian, J., Ao, Y. H., Wang, C., and Hou, J. (2018). Phosphate group grafted twinned BiPO$_4$ with significantly enhanced photocatalytic activity: synergistic effect of improved charge separation efficiency and redox ability. *Appl. Catal. B Environ.* 234, 90–99. doi: 10.1016/j.apcatb.2018.04.036

Han, W., Liu, Z., Li, Y., Fan, X., Zhang, F., Zhang, G., et al. (2018). The promoting role of different carbon allotropes cocatalysts for semiconductors in photocatalytic energy generation and pollutants degradation. *Front. Chem.* 5:84. doi: 10.3389/fchem.2017.00084

He, S., Hou, P., Petropoulos, E., Feng, Y., Yu, Y., Xue, L., et al. (2018). High efficient visible-light photocatalytic performance of Cu/ZnO/rGO nanocomposite for decomposing of aqueous ammonia and treatment of domestic wastewater. *Front. Chem.* 6:219. doi: 10.3389/fchem.2018.00219

Hu, J. L., Wu, X. X., Huang, C. J., Fan, W. J., and Qiu, X. Q. (2016). Visible light photocatalytic activity induced by Rh(III) modification on the surface of BiOCl. *Appl. Surf. Sci.* 387, 45–50. doi: 10.1016/j.apsusc.2016.06.075

Katsumata, K., Okazaki, S., Cordonier, C. E., Shichi, T., Sasaki, T., and Fujishima, A. (2010). Preparation and characterization of self-cleaning glass for vehicle with niobia nanosheets. *ACS Appl. Mater. Interfaces* 2, 1236–1241. doi: 10.1021/am100091f

Kuang, P. Y., Su, Y. Z., Chen, G. F., Luo, Z., Xing, S. Y., Li, N., et al. (2015). g-C$_3$N$_4$ decorated ZnO nanorod arrays for enhanced photoelectrocatalytic performance. *Appl. Surf. Sci.* 358, 296–303. doi: 10.1016/j.apsusc.2015.08.066

Kumar, S., Khanchandani, S., Thirumal, M., and Ganguli, A. K. (2014). Achieving enhanced visible-light-driven photocatalysis using type-II NaNbO$_3$/CdS core/shell heterostructures. *ACS Appl. Mater. Interfaces* 6, 13221–13233. doi: 10.1021/am503055n

Li, G., Kako, T., Wang, D., Zou, Z., and Ye, J. (2008). Synthesis and enhanced photocatalytic activity of NaNbO$_3$ prepared by hydrothermal and polymerized complex methods. *J. Phys. Chem. Solids* 69, 2487–2491. doi: 10.1016/j.jpcs.2008.05.001

Li, G., Yi, Z., Bai, Y., Zhang, W., and Zhang, H. (2012a). Anisotropy in photocatalytic oxidization activity of NaNbO$_3$ photocatalyst. *Dalton Trans.* 41, 10194–10198. doi: 10.1039/c2dt30593c

Li, G. Q. (2010). Photocatalytic properties of NaNbO$_3$ and Na$_{0.6}$Ag$_{0.4}$NbO$_3$ synthesized by polymerized complex method. *Mater. Chem. Phys.* 121, 42–46. doi: 10.1016/j.matchemphys.2009.12.032

Li, P., Ouyang, S., Xi, G., Kako, T., and Ye, J. H. (2012b). The effects of crystal structure and electronic structure on photocatalytic H$_2$ evolution and CO$_2$ reduction over two phases of perovskite-structured NaNbO$_3$. *J. Phys. Chem. C* 116, 7621–7628. doi: 10.1021/jp210106b

Li, P., Ouyang, S. X., Zhang, Y. J., Kako, T., and Ye, J. H. (2013). Surface-coordination-induced selective synthesis of cubic and orthorhombic NaNbO$_3$ and their photocatalytic properties. *J. Mater. Chem. A* 1, 1185–1191. doi: 10.1039/C2TA00260D

Li, P., Xu, H., Liu, L. Q., Kako, T., Umezawa, N., Abe, H., et al. (2014). Constructing cubic–orthorhombic surface-phase junctions of NaNbO$_3$ towards significant enhancement of CO$_2$ photoreduction. *J. Mater. Chem. A* 2, 5606–5609. doi: 10.1039/C4TA00105B

Li, Q., Li, X., Wageh, S., Al-Ghamdi, A. A., and Yu, J. (2015). CdS/Graphene nanocomposite photocatalysts. *Adv. Energy Mater.* 5:1500010. doi: 10.1002/aenm.201500010

Li, S., Hu, S., Jiang, W., Liu, Y., Liu, Y., Zhou, Y. T., et al. (2018). Ag$_3$VO$_4$ nanoparticles decorated Bi$_2$O$_2$CO$_3$ micro-flowers: an efficient visible-light-driven photocatalyst for the removal of toxic contaminants. *Front. Chem.* 6:255. doi: 10.3389/fchem.2018.00255

Liu, M. R., Hong, Q. L., Li, Q. H., Du, Y. H., Zhang, H. X., Chen, S. M., et al. (2018). Cobalt boron imidazolate framework derived cobalt nanoparticles encapsulated in B/N codoped nanocarbon as efficient bifunctional electrocatalysts for overall water splitting. *Adv. Funct. Mater.* 28:1801136. doi: 10.1002/adfm.201801136

Liu, Q. Q., Chai, Y. Y., Zhang, L., Ren, J., and Dai, W. L. (2016). Highly efficient Pt/NaNbO$_3$ nanowire photocatalyst: Its morphology effect and application in water purification and H$_2$ production. *Appl. Catal. B Environ.* 205, 505–513. doi: 10.1016/j.apcatb.2016.12.065

Liu, W. W., Qiao, L. L., Zhu, A. Q., Liu, Y., and Pan, J. (2017a). Constructing 2D BiOCl/C3N4 layered composite with large contact surface for visible-light-driven photocatalytic degradation. *Appl. Surf. Sci.* 426, 897–905. doi: 10.1016/j.apsusc.2017.07.225

Liu, W. W., Shang, Y. Y., Zhu, A. Q., Tan, P. F., Liu, Y., Qiao, L. L., et al. (2017b). Enhanced performance of doped BiOCl nanoplates for photocatalysis: understanding from doping insight into improved spatial carrier separation. *J. Mater. Chem. A* 5:12542–12549. doi: 10.1039/C7TA02724A

Lv, J., Kako, T., Li, Z. S., Zou, Z. G., and Ye, J. H. (2010). Synthesis and photocatalytic activities of NaNbO3 rods modified by In$_2$O$_3$ nanoparticles. *J. Phys. Chem. C* 114, 6157–6162. doi: 10.1021/jp906550t

Ma, W., Chen, L., Zhu, Y. Z., Dai, J. D., Yan, Y. S., and Li, C. X. (2016). Facile synthesis of the magnetic BiOCl/ZnFe$_2$O$_4$ heterostructures with enhanced photocatalytic activity under visible-light irradiation. *Colloids Surfaces A Physicochem Eng. Aspects.* 508, 135–141. doi: 10.1016/j.colsurfa.2016.08.066

Ma, Y. C., Chen, Z. W., Qu, D., and Shi, J. S. (2016). Synthesis of chemically bonded BiOCl@Bi$_2$WO$_6$ microspheres with exposed (020) Bi$_2$WO$_6$ facets and their enhanced photocatalytic activities under visible light irradiation. *Appl. Surf. Sci.* 361, 63–71. doi: 10.1016/j.apsusc.2015.11.130

Mao, D. J., Yu, A. Q., Ding, S. S., Wang, F., Yang, S. G., Sun, C., et al. (2016). One-pot synthesis of BiOCl half-shells using microemulsion droplets astemplates with highly photocatalytic performance for the degradation of ciprofloxacin. *Appl. Surf. Sci.* 389, 742–750. doi: 10.1016/j.apsusc.2016.07.178

Qian, J., Xue, Y., Ao, Y. H., Wang, P. F., and Wang, C. (2018). Hydrothermal synthesis of CeO$_2$/NaNbO$_3$ composites with enhanced photocatalytic performance. *Chin. J. Catal.* 39, 682–692. doi: 10.1016/S1872-2067(17)62975-9

Rajeshwar, K., de Tacconi, N. R., and Chenthamarakshan, C. R. (2001). Semiconductor-based composite materials: preparation, properties, and performance. *Chem. Mater.* 13, 2765–2782. doi: 10.1021/cm010254z

Saito, K., and Kudo, A. (2013). Fabrication of highly crystalline SnNb$_2$O$_6$ shell with a visible-light response on a NaNbO$_3$ nanowire core. *Inorg. Chem.* 52, 5621–5623. doi: 10.1021/ic4002175

Shang, M., Wang, W. Z., Zhang, L., and Zhou, L. (2009). 3D Bi$_2$WO$_6$/TiO$_2$ hierarchical heterostructure: controllable synthesis and enhanced visible photocatalytic degradation performances. *J. Phys. Chem. C* 113, 14727–14731. doi: 10.1021/jp9045808

Shi, H. F., Chen, G. Q., Zhang, C. L., and Zou, Z. G. (2014b). Polymeric g-C$_3$N$_4$ coupled with NaNbO$_3$ nanowires toward enhanced photocatalytic reduction of CO$_2$ into renewable fuel. *ACS Catal.* 4, 3637–3643. doi: 10.1021/cs500848f

Shi, H. F., Chen, G. Q., and Zou, Z. G. (2014a). Platinum loaded NaNbO$_3$-xNx with nanostep surface nanostructures toward enhanced visible-light photocatalytic activity. *Appl. Catal. B Environ.* 156, 378–384. doi: 10.1016/j.apcatb.2014.03.036

Shifu, C., Ji, L., Tang, W. M., and Fu, X. L. (2013). Fabrication, characterization and mechanism of a novel Z-scheme photocatalyst NaNbO$_3$/WO$_3$ with enhanced photocatalytic activity. *Dalton Trans.* 42, 10759–10768. doi: 10.1039/c3dt50699a

Song, C. J., Fan, M. S., Hu, B., Chen, T. J., Wang, L. P., and Shi, W. D. (2015). Synthesis of a g-C$_3$N$_4$-sensitized and NaNbO$_3$-substrated II-type heterojunction with enhanced photocatalytic degradation activity. *Cryst. Eng. Comm.* 17, 4575–4583. doi: 10.1039/C5CE00622H

Sun, M., Yan, Q., Shao, Y., Wang, C. Q., Yan, T., Ji, P. G., et al. (2017). Facile fabrication of BiOI decorated NaNbO$_3$ cubes: a p–n junction photocatalyst with improved visible-light activity. *Appl. Surf. Sci.* 416, 288–295. doi: 10.1016/j.apsusc.2017.04.136

Wang, D. H., Gao, G. Q., Zhang, Y. W., Zhou, L. S., Xu, A. W., and Chen, W. (2012). Nanosheet-constructed porous BiOCl with dominant {001} facets for superior photosensitized degradation. *Nanoscale* 4, 7780–7785. doi: 10.1039/c2nr32533k

Wang, H., Zhang, W. D., Li, X. W., Li, J. Y., Cen, W. L., Li, Q. Y., et al. (2018). Highly enhanced visible light photocatalysis and *in situ* FT-IR studies on Bi metal@defective BiOCl hierarchical microspheres. *Appl. Catal. B Environ.* 225, 218–227. doi: 10.1016/j.apcatb.2017.11.079

Xu, Y., Mo, Y. P., Tian, J., Wang, P., Yu, H. G., and Yu, J. G. (2016). The synergistic effect of graphitic N and pyrrolic N for the enhanced photocatalytic performance of nitrogen-doped graphene/TiO2 nanocomposites. *Appl. Catal. B Environ.* 181, 810–817. doi: 10.1016/j.apcatb.2015.08.049

Yan, M., Hua, Y. Q., Zhu, F. F., Gu, W., Jiang, J. H., Shen, H. Q., et al. (2017). Fabrication of nitrogen doped graphene quantum dots-BiOI/MnNb$_2$O$_6$ p–n junction photocatalysts with enhanced visible light efficiency in photocatalytic degradation of antibiotics. *Appl. Catal. B Environ.* 202, 518–527. doi: 10.1016/j.apcatb.2016.09.039

Yang, Y., Zhang, Q., Zhang, R. Y., Ran, T., Wan, W. C., and Zhou, Y. (2018). Compressible and recyclable monolithic g-C$_3$N$_4$/melamine sponge: a facile ultrasonic-coating approach and enhanced visible-light photocatalytic activity. *Front. Chem.* 6:156. doi: 10.3389/fchem.2018.00156

Ye, L. Q., Su, Y. R., Jin, X. L., Xie, H., and Zhang, C. (2014). Recent advances in BiOX (X = Cl, Br and I) photocatalysts: synthesis modification, facet effects and mechanisms. *Environ. Sci. Nano.* 1, 90–112. doi: 10.1039/c3en00098b

Yu, H. G., Xiao, P., Tian, J., Wang, F. Z., and Yu, J. G. (2016). Phenylamine-functionalized rGO/TiO$_2$ photocatalysts: spatially separated adsorption sites and tunable photocatalytic selectivity. *ACS Appl. Mat. Interfaces* 8, 29470–29477. doi: 10.1021/acsami.6b09903

Yuan, X. Z., Wang, H., Wang, J. J., Zeng, G. M., Chen, X. H., Wu, Z. B., et al. (2018). Near-infrared-driven Cr (VI) reduction in aqueous solution based on a MoS$_2$/Sb$_2$S$_3$ photocatalyst. *Catal. Sci. Technol.* 8, 1545–1554. doi: 10.1039/C7CY02531A

Zhang, B. B., Zhang, D. F., Xi, Z. S., Wang, P. F., Pu, X. P., Shao, X., et al. (2017). Synthesis of Ag$_2$O/NaNbO$_3$ p-n junction photocatalysts with improved visible light photocatalytic activities. *Sep. Purification Technol.* 178, 130–137. doi: 10.1016/j.seppur.2017.01.031

Zhang, J. F., Wageh, S., Al-Ghamdic, A., and Yu, J. G. (2016). New understanding on the different photocatalytic activity of wurtzite and zinc-blende CdS. *Appl. Catal. B Environ.* 192, 101–107. doi: 10.1016/j.apcatb.2016.03.058

Zhang, J. Y., Xiao, F. X. (2017). Modulation of interfacial charge transfer by self-assembly of single-layer graphene enwrapped one-dimensional semiconductors toward photo redox catalysis. *J. Mat. Chem. A.* 5, 23681–23693. doi: 10.1039/C7TA08415C

Zhang, W. D., Liu, X. L., Dong, X. A., Dong, F., and Zhang, Y. X. (2017a). Facile synthesis of Bi$_{12}$O$_{17}$Br$_2$ and Bi$_4$O$_5$Br$_2$ nanosheets: *in situ* DRIFTS investigation of photocatalytic NO oxidation conversion pathway. *Chin. J. Catal.* 38, 2030–2038. doi: 10.1016/S1872-2067(17)62941-3

Zhang, W. D., Zhao, Z. W., Dong, F., and Zhang, Y. X. (2017b). Solvent-assisted synthesis of porous g-C$_3$N$_4$ with efficient visible-light photocatalytic performance for NO removal. *Chin. J. Catal.* 38, 372–378. doi: 10.1016/S1872-2067(16)62 585-8

Zhong, Y. X., Liu, Y. H., Wu, S., Zhu, Y., Chen, H. B., and Yu, X. (2018). Facile fabrication of BiOI/BiOCl immobilized films with improved visible light photocatalytic performance. *Front. Chem.* 6:58. doi: 10.3389/fchem.2018.00058

Zhou, T. H., Du, Y. H., Wang, D. P., Yin, S. M., Tu, W. G., Chen, Z., et al. (2017). Phosphonate-based metal-organic framework derived Co-P-C hybrid as an efficient electrocatalyst for oxygen evolution reaction. *ACS Catal.* 7:6000–6007. doi: 10.1021/acscatal.7b 00937